Naval Research Laboratory

Washington, DC 20375-5320

NRL/MR/6750--10-9237

A Note on Determining the Electron Distribution Function from RF Impedance Probe Measurements

D.N. WALKER

Global Strategies Group, Inc.
Crofton, Maryland

R.F. FERNSLER
D.D. BLACKWELL
W.E. AMATUCCI

Charged Particle Physics Branch
Plasma Physics Division

February 17, 2010

REPORT DOCUMENTATION PAGE

Form Approved
OMB No. 0704-0188

1. REPORT DATE *(DD-MM-YYYY)*	**2. REPORT TYPE**	**3. DATES COVERED** *(From - To)*
17-02-2010	Memorandum Report	

4. TITLE AND SUBTITLE

A Note on Determining the Electron Distribution Function from RF Impedance Probe Measurements

5a. CONTRACT NUMBER

5b. GRANT NUMBER

5c. PROGRAM ELEMENT NUMBER

6. AUTHOR(S)

D. N. Walker,* R. F. Fernsler, D. D. Blackwell, and W. E. Amatucci

5d. PROJECT NUMBER
67-9872-00

5e. TASK NUMBER

5f. WORK UNIT NUMBER

7. PERFORMING ORGANIZATION NAME(S) AND ADDRESS(ES)

Naval Research Laboratory
4555 Overlook Avenue, SW
Washington, DC 20375-5320

*Global Strategies Group (North America) Inc.
2200 Defense Highway
Crofton, MD 21114

8. PERFORMING ORGANIZATION REPORT NUMBER

NRL/MR/6750--10-9237

9. SPONSORING / MONITORING AGENCY NAME(S) AND ADDRESS(ES)

Office of Naval Research
One Liberty Center
875 North Randolph Street
Arlington, VA 22203-1995

10. SPONSOR / MONITOR'S ACRONYM(S)

ONR

11. SPONSOR / MONITOR'S REPORT NUMBER(S)

12. DISTRIBUTION / AVAILABILITY STATEMENT

Approved for public release; distribution is unlimited.

13. SUPPLEMENTARY NOTES

14. ABSTRACT

We have demonstrated in earlier work the usefulness of a network analyzer in plasma diagnostics using spherical probes in the thin sheath limit. The rf signal applied to the probe by the network analyzer is small in magnitude compared to probe bias voltages and the instrument returns both real and imaginary parts of the complex plasma impedance as a function of frequency for given bias voltages. This information can be used to determine sheath resistance, sheath density profiles, and a technique for measuring electron temperature.

15. SUBJECT TERMS

Plasma sheath
Collisionless plasma
Plasma impedance
Plasma potential

16. SECURITY CLASSIFICATION OF:			**17. LIMITATION OF ABSTRACT**	**18. NUMBER OF PAGES**	**19a. NAME OF RESPONSIBLE PERSON**
a. REPORT	**b. ABSTRACT**	**c. THIS PAGE**			Richard F. Fernsler
Unclassified	Unclassified	Unclassified	UL	15	**19b. TELEPHONE NUMBER** *(include area code)* (202) 767-6786

Standard Form 298 (Rev. 8-98)
Prescribed by ANSI Std. Z39.18

TABLE OF CONTENTS

I. Introduction

We have used rf techniques with plasma probes in laboratory experiments to demonstrate the existence of collisionless resistance in the sheath of a spherical probe[1], shown that this leads to a method of finding the electron sheath density profile[2], and proposed a method of measuring electron temperature.[3] In the most recent work we demonstrated a method of determining plasma potential.[4] In the present work we show that the electron distribution function can be determined from a 1st derivative of the inverse ac resistance as covered below. The usual convention requires a 2nd derivative of collected electron current with respect to applied voltage bias in the neighborhood of the plasma potential since it is only there that electron and total probe collected current are nearly the same.

II. Determining f(ε)

Druyvesteyn[5] showed that the electron energy distribution function, *f(ε)*, for a negatively biased probe in a plasma is given by,

$$f(\varepsilon) = \frac{4}{e^3 A_p}\sqrt{\frac{m_e \varepsilon}{2}}\left(\frac{d^2 I_e}{dV_p^2}\right)_{eV_p=-\varepsilon} \tag{1}$$

where A_p is the probe area, I_e is the electron current collected by the probe, m_e is electron mass, and V_p is the bias voltage with respect to plasma potential, φ_p, and ε is the energy.

Total current collected by a Langmuir probe, I_p, will include both electron current in addition to any negative ion current, along with positive ion current. Because of this d^2I_e/dV_p^2 can only be set equal to d^2I_p/dV_p^2 for small biases, V_p. This implies that f(ε) can be estimated for low energies but not high ones. Common procedure relies on assuming a form for the ion current, which can be subtracted from the total to give I_e. As this form for I_p is often arbitrary and not well justified, we have outlined in recent work[6] a method of obtaining more accurate estimates.

A better solution would involve measuring I_e directly without the necessity of obtaining it from the total collected current thus eliminating ion current contributions altogether. As discussed above when applying a small-amplitude rf signal to a probe, the ions contribute little to the total current if the applied frequency, ω, is such that $\omega_{pi} << \omega$ where ω_{pi} is the ion plasma frequency. In addition if $\omega < \omega_{pe}(r_0)$ with $\omega_{pe}(r_0)$ the electron plasma frequency at the probe surface, r_0., we avoid electron resonance effects discussed in an earlier paper[1], and *f(ε)* can be expressed as

$$f(\varepsilon) = \frac{4}{e^3 A_p}\sqrt{\frac{m_e \varepsilon}{2}}\left(\frac{dR_{ac}^{-1}}{dV_p}\right)_{eV_p=-\varepsilon} \tag{2}$$

where R_{ac} is the ac resistance.[3] The justification for replacing d^2I_e/dV_p^2 with dR_{ac}^{-1}/dV_p

Manuscript approved December 7, 2009.

is covered in the Appendix.

III. Brief Description of Experimental Procedure

We refer the reader interested in the experimental details to earlier works[1,4] and only provide an outline of that same description here.

The experiments we describe here were conducted using rwo small stainless steel spheres of 1.25 cm and 2.54 cm radius which were connected to an HP8735D Network Analyzer through 50 Ω coaxial cable which provides the driving signal. This arrangement including the chamber, analyzer and the coupling circuitry is shown schematically in Figures 1 and 2. The spheres were mounted on a 1/4 inch diameter ceramic and steel support which is connected to 1/4 inch diameter semi-rigid copper 50 Ohm coaxial cable.

For all of the experiments, the determination of plasma impedance depends upon the network analyzer measurement of the complex reflection coefficient, Γ(ω). From this measurement the analyzer returns as separate outputs *Re* $Z_{ac}(\omega)$ and *Im* $Z_{ac}(\omega)$ where,

$$Z_{ac}(\omega) = Z_0[\frac{1+\Gamma(\omega)}{1-\Gamma(\omega)}] \tag{3}$$

and Z_0 (=50 Ω) is the internal impedance of the analyzer. We also note that the ratio of reflected-to-total power is given by,

$$|\Gamma|^2 = \frac{P_r}{P_0} \tag{4}$$

where $P_0 = P_R + P_T$ with P_R and P_T the reflected and transmitted powers, respectively. (The quantity 1- $|\Gamma|^2$ is the normalized transmitted power and this output is also available).

IV. Results for f(ε) and Comparison to Langmuir Probe Data

Using Eq. (2) we plot as examples $f(\varepsilon)$ for two probes of radius 1.25 cm (Figure 4), and 2.54 cm (Figure 5). For each of the plots we have determined the average energy, E_{av}, and the electron density, n_e, from the usual integrals over energy of $\varepsilon f(\varepsilon)$ and $f(\varepsilon)$, respectively. The electron temperature is estimated as $T_e \approx 2/3\ E_{av}$. The plots each show good correspondence between the conventional Langmuir probe results and those of the method presented here.

V. Summary

We have presented a method of determining the electron distribution function using techniques developed over the past three years in studies of rf impedance probes using very small amplitude signals compared to bias levels or typical plasma potential magnitudes. For this reason our technique is non-perturbative to the existing plasma-probe interface and is unaffected by the presence of probe contamination.

VI. Appendix

A.1 The origin of Eq. (2)

The total ac impedance, Z_{ac}, of a circuit whose model includes a parallel combination of C_{ac},R_{ac} to represent the sheath, in series with a bulk plasma inductance, L_p, is given by,

$$Z_{ac}(\omega) = Z_{ac,s}(\omega) + i\omega L_p = \frac{1}{i\omega C_{ac} + R_{ac}^{-1}} + i\omega L_p \tag{A.1}$$

where $Z_{ac,s}(\omega)$ is used to denote sheath impedance, C_{ac} is sheath ac capacitance discussed below and,

$$L_p = \int_{r_s}^{\infty} dr \frac{m_e}{4\pi r^2 e^2 n_e(r)}. \tag{A.2}$$

with r_s denoting sheath radius. (In earlier work[3], we included a sheath inductance but this term, which considerably complicates the solution, was found to be negligible for the frequencies we consider.) After some algebra it can be shown that,

$$R_{ac} = \frac{\mathrm{Re}(Z_{ac})^2 + (\omega L_p - \mathrm{Im}(Z_{ac}))^2}{\mathrm{Re}(Z_{ac})} \tag{A.3}$$

and,

$$C_{ac} = \frac{\omega L_p - \mathrm{Im}(Z_{ac})}{\omega(\omega L_p - \mathrm{Im}(Z_{ac}))^2 + \omega\,\mathrm{Re}(Z_{ac})^2} \tag{A.4}$$

Eliminating L_p from Eqs. (A.3) and (A.4) we are able to write[3],

$$\mathrm{Re}(Z_{ac}) = \frac{R_{ac}}{1 + (\omega R_{ac} C_{ac})^2} \tag{A.5}$$

where,

$$R_{ac} = (\frac{dI_e}{dV_p})^{-1} = \frac{1}{4\pi\varepsilon_0}\left(\frac{\lambda_D}{r_0}\right)^2 e^{-eV_0/T_e}\sqrt{\frac{2\pi m_e}{T_e}} \tag{A.6}$$

and we require that $\omega_{pi} << \omega < \omega_{pe}(r_0)$ with $\omega_{pe}(r_0)$ the electron plasma frequency at the probe surface, r_0. V_p is taken as the dc bias with respect to plasma potential, C_{ac} is sheath capacitance, λ_D is Debye length, and m_e,T_e are electron mass and temperature, respectively. Eqs. (A.3) and (A.4) arise from the circuit representation of the probe plasma interaction whereas Eq. (A.6) is based on physical theory which includes an assumption of Boltzmann electrons and ignores ion current contributions.[3] Unlike the case where a very low frequency is applied ($\omega < \omega_{pi}$, ω_{pe}), the lower bound to the frequency range above avoids most ion contributions to the total ac current. For the upper bound, there will be no contribution from collisionless resistance (CR) (or resonance effects) covered in the original work in this series.[1] Eq. (A.6) and the reasoning which produces it are the basis of the transition from the Druystevn equation seen in Eq. (4) to the form in Eq (5).

If Eq. (A.5) is solved for R_{ac}, we obtain,

$$R_{ac} = \frac{1-\sqrt{1-4\omega^2\,\mathrm{Re}(Z_{ac})^2 C_{ac}^2}}{2\omega^2 C_{ac}^2\,\mathrm{Re}(Z_{ac})} \tag{A.7}$$

And so, to the extent that $(\omega \mathrm{Re}(Z_{ac})C_{ac})^2 << 1$ in Eq (A.5) , $R_{ac} \sim \mathrm{Re}(Z_{ac})$ Therefore R_{ac} has a minimum at φ_p. This will generally hold true for small biases near φ_p and the frequencies and sheath sizes applicable in our experiment, *i.e.*, frequencies no larger than approximately $0.1\omega_{pe}$, and probe radii no larger than 2.54 cm.

We then have at $V_p = \varphi_p$,

$$\frac{dR_{ac}}{dV_p} = -R_{ac}^2\left(\frac{d^2 I_e}{dV_p^2}\right) = 0 \tag{A.8}$$

and finally,

$$\left.\frac{d\,\mathrm{Re}(Z_{ac})}{dV_p}\right|_{V_p=\phi_p} \simeq 0 \tag{A.9}$$

Because of this we can plot the network analyzer output of $Re(Z_{ac})$ versus applied bias for frequencies in the range specified. Each of these curves will then show a minimum at $V_p = \varphi_p$. An example of these plots from previous work[4] for the two probes is shown in Fig. (3). Due to the dependence of $f(\varepsilon)$ on dR_{ac}^{-}/dV_p seen in Eq (2) we are able to construct $f(\varepsilon)$ in the vicinity of φ_p for small negative bias voltages. This is the basis of Figs (4) and (5)

A.2 Determining C_{ac}

Eq (A.4) which relies almost entirely on experimental data can be used to determine *ac capacitance*, C_{ac}, from Re(Z_{ac}), Im(Z_{ac}), and L_p as found from Eq (A.2) where $n_e(r)$ is determined from solution of the Poisson equation. Note that the lower integration boundary is the sheath edge, r_s. We make a distinction here between C_{ac} and *dc capacitance*, C_{dc}. This can be seen when realizing that we are applying a small rf signal to a biased probe. The total charge on the probe may then be expressed,

$$Q(t) = Q_{dc} + Q_{ac} e^{i\omega t} \tag{A.10}$$

where $Q_{ac} << Q_{dc}$ and therefore to lowest order,

$$Q_{ac} = V_{ac} \left. \frac{dQ_{dc}}{dV_{dc}} \right|_{dc} \quad with, \;\; C_{ac} = \frac{Q_{ac}}{V_{ac}} = 4\pi r_0^2 \varepsilon_0 \left. \frac{dE_r(r_0)}{dV_{dc}} \right|_{V_{dc}} . \tag{A.11}$$

V_{dc} is the potential with respect to the bulk plasma and $V_{ac} << V_{dc}$ is the ac voltage. The expression for C_{ac} in Eq. (A.11) arises from the fact that, for a spherical probe in a bulk plasma,

$$Q_{dc} = 4\pi r_0^2 \varepsilon_0 E_r(r_0) \;\; and, \;\; C_{dc} = \frac{Q_{dc}}{V_{dc}}. \tag{A.12}$$

Eq (A.12) results from observing that the electric field vanishes far from the probe and therefore the probe and the bulk plasma contain equal amounts of charge. Earlier work[6] can provide $E_r(r_0)$, the electric field at the surface, as a function of the applied bias. From this model, it is possible to numerically fit $E_r(r_0)$ as a function of V_{dc} and to determine $dE_r(r_0)/dV_{dc}$ and hence C_{ac}. For a typical case we find that C_{ac} is similar to C_{dc} with C_{ac} being generally larger. However, the magnitudes of those differences do not substantially alter the results here, *i.e.*, the effect on the determination of plasma potential and $f(\varepsilon)$ is insignificant for the frequency ranges, probe sizes, and magnitudes of $Re(Z_{ac})$ near plasma potential. This can be seen in the denominator of Eq. (A.5) where the term $(\omega R_{ac} C_{ac})^2 << 1$ is typical for these parameter regimes. Also, comparison to Langmuir probe measurements is largely consistent with the plasma parameters (N_e, T_e) calculated from the determination of $f(\varepsilon)$ using the method outlined.

It is also useful to note that C_{dc} can be be estimated in two ways from vacuum values. Using either as an estimate of C_{ac} does not greatly affect the results of the determinations of $f(\varepsilon)$. However since both are estimates of C_{dc} they are not justified on physical grounds as a correct representation of C_{ac}. One method uses the vacuum capacitance of an isolated sphere, C_0, whereas another uses the vacuum capacitance of two concentric spheres, the outer defined by the sheath edge. The vacuum estimates are also useful as benchmarks and for comparison to the results of Eq. (A.7), *i.e.*, using the numerical model for a sphere of radius $10\lambda_{De}$ for example, yields a typical ratio $2.5 < C_{dc}/C_0 < 3.7$ when only applying a dc bias. In this case, the lower bound corresponds to

plasma potential, V_p, and the upper, near 1 V removed from V_p. In the second case r_s is estimated from a solution of the Poisson equation. This solution proceeds by uniquely determining bulk electron density, n_0 , from the resonance in Re(Z_{ac}) and the zero crossing of Im(Z_{ac}). With this information we are able to estimate r_s with only an assumption as to the approximate electron temperature T_e. This is possible because the sheath width is largely independent of T_e for this model.[3] The Poisson equation is solved by specifying these boundary conditions at the sheath edge and integrating inward to the final bias which produces a given r_s and therefore the two-sphere vacuum capacitance. This method produces an estimate which is always larger than that of an isolated sphere but is increasingly unphysical when approaching the limit of a vanishing sheath. In an intermediate range of bias voltages (i.e., for sufficiently large sheaths) this method is closer to the results of the correct calculation of C_{dc} and varies as a function of bias.

An advantage to having the analytic expression for C_{ac} of Eq. (A.11) is that it is possible compare to experimental-based results obtained through Eq (A.4) to a more realistic theoretical basis than the vacuum estimations described in the last paragraph. This can be done for example by using the Poisson equation-based calculation described above to find $E_r(r_0)$ and hence by differentiation, C_{ac}. This is planned in future work which will address the issue in more detail.

VII. Figure Captions

Figure (1) – A photograph of the present NRL Space Physics Simulation Chamber showing magnetic field coils and two separate experimental areas separated by a large gate valve providing either experimental coupling between the two or isolation for separate experimentation. The results presented in this work were performed in the larger section surrounded by five magnetic field coils toward the rear of the photograph.

Figure (2) – A schematic representation of the Network Analyzer and coupling circuitry necessary for the swept frequency analyses of the spherical impedance probes. The Analyzer returns a representation of the signal reflected from the plasma and provides plasma complex impedance, The circuitry shown indicates both the application of the small non-perturbative analyzer signal in addition to the dc bias applied to the probes.

Figure (3) – A plot of the $Re(Z_{ac})$ for frequency scans varying from 11 to 20 MHz returned by the Network Analyzer vs applied bias voltage for the 25.4 mm radius sphere. For this run the plasma potential determined from Langmuir probe data, $\varphi_p \sim 1.5$ V, plasma temperature, $T_e \sim 0.4$ eV and electron density, $n_e \sim 10^8$ cm^{-3}.

Figure (4) – A plot of the electron distribution function $f(\varepsilon)$ vs applied probe bias for the 2.54 cm probe for an analyzer sweep frequency of 3 MHz. From $f(\varepsilon)$ we find by integration that $n_e = 1.23 \times 10^8$ cm^{-3} and $T_e = 0.38$ eV . This is to be compared to a Langmuir probe determination of $n_e \approx 1 \times 10^8$ cm^{-3} and $T_e \approx 0.4$ eV

Figure (5) – A plot of the electron distribution function $f(\varepsilon)$ vs applied probe bias for the 1.25 cm probe for an analyzer sweep frequency of 4 MHz. From $f(\varepsilon)$ we find by integration that $n_e = 3.4 \times 10^7$ cm^{-3} and $T_e = 0.74$ eV . This is to be compared to a Langmuir probe determination of $n_e \approx 4 \times 10^7$ cm^{-3} and $T_e \approx 0.8$ eV

VIII. References

[1]D.N. Walker, R.F. Fernsler, D.D. Blackwell, W.E. Amatucci, and S.J. Messer, *Phys. Plasmas* **13**, 032108 (2006)

[2]D.N. Walker, R.F. Fernsler, D.D. Blackwell, W.E. Amatucci, *NRL Memorandum Report*, **6750-07-9033** (2007)

[3]D.N. Walker, R.F. Fernsler, D.D. Blackwell, W.E. Amatucci, *Phys. Plasmas* **15**, 123506 (2008)

[4]D.N. Walker, R.F. Fernsler, D.D. Blackwell, W.E. Amatucci, *NRL Memorandum Report*, **6750-09-9197** (2009)

[5]M.J. Druyvesteyn, *Physica* **10**, 69, 1930

[6]R.F. Fernsler, *Plasma Sources Sci. and Technol*, **18**, 014012 (2009)

IX. Figures

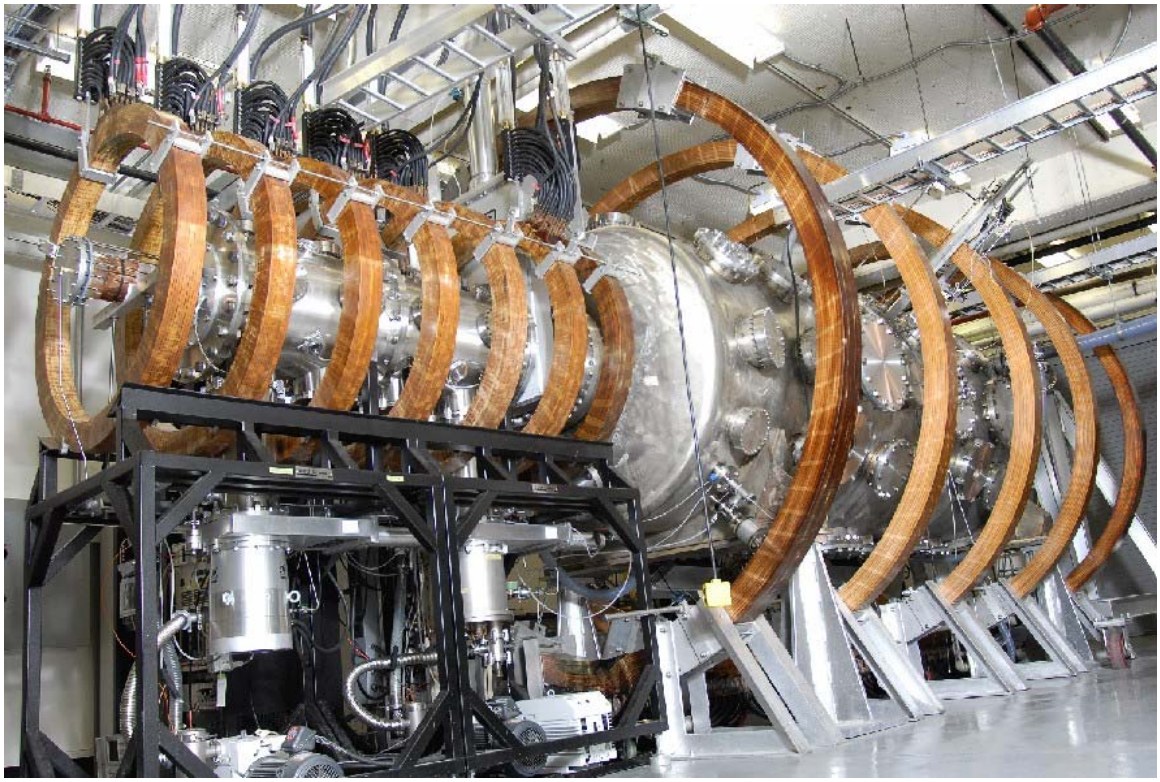

Figure 1

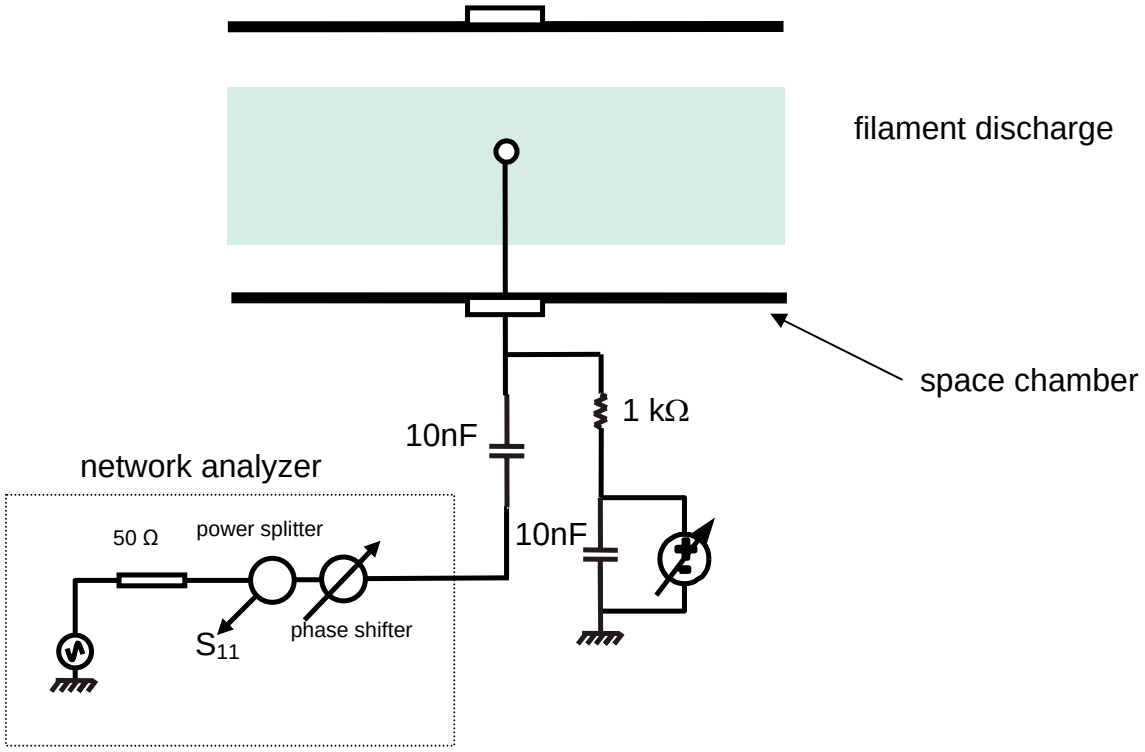
filament discharge
space chamber
1 kΩ
10nF
network analyzer
10nF
50 Ω
power splitter
S11
phase shifter

Figure 2

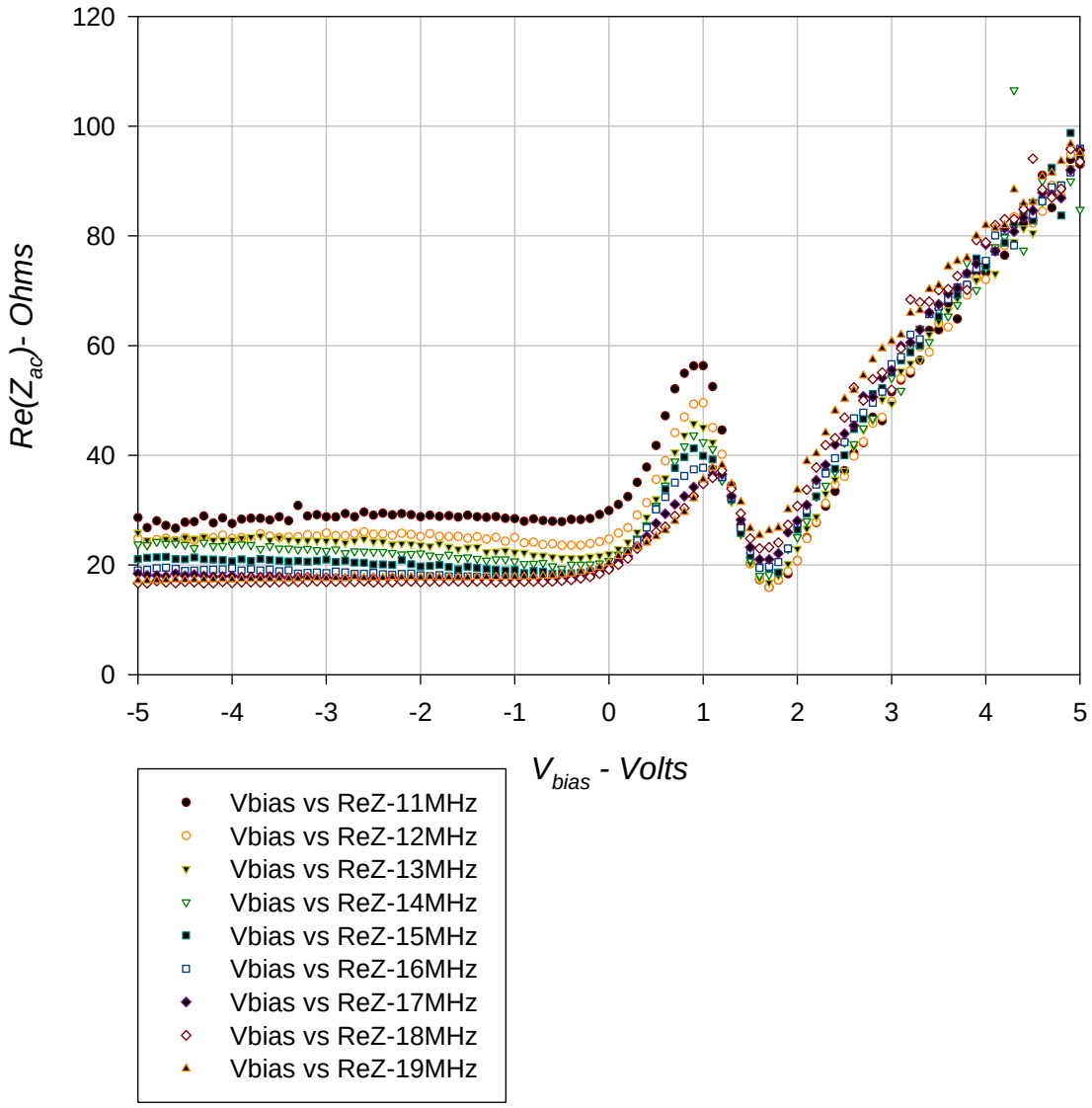
120
100
80
60
40
20
0
-5
-4
-3
-2
-1
0
1
2
3
4
5
Re(Z_ac)- Ohms
V_bias - Volts
Vbias vs ReZ-11MHz
Vbias vs ReZ-12MHz
Vbias vs ReZ-13MHz
Vbias vs ReZ-14MHz
Vbias vs ReZ-15MHz
Vbias vs ReZ-16MHz
Vbias vs ReZ-17MHz
Vbias vs ReZ-18MHz
Vbias vs ReZ-19MHz

Figure 3

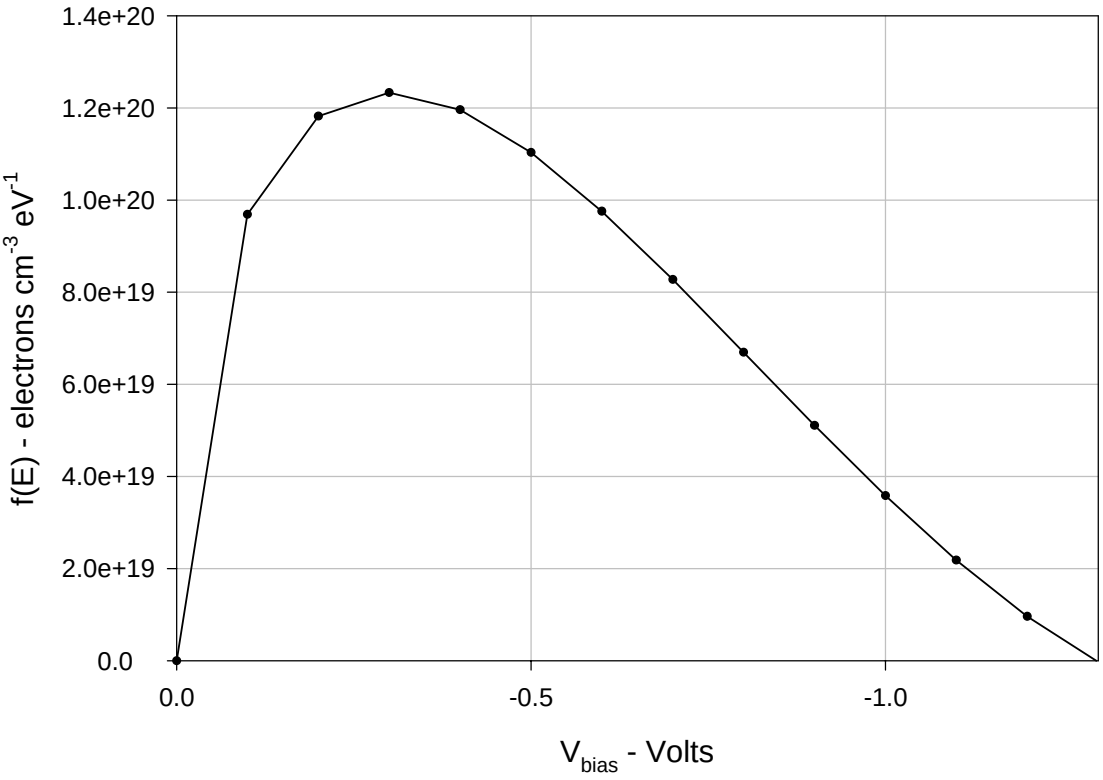
1.4e+20
1.2e+20
1.0e+20
8.0e+19
6.0e+19
4.0e+19
2.0e+19
0.0
f(E) - electrons cm-3 eV-1
0.0
-0.5
-1.0
Vbias - Volts

Figure 4

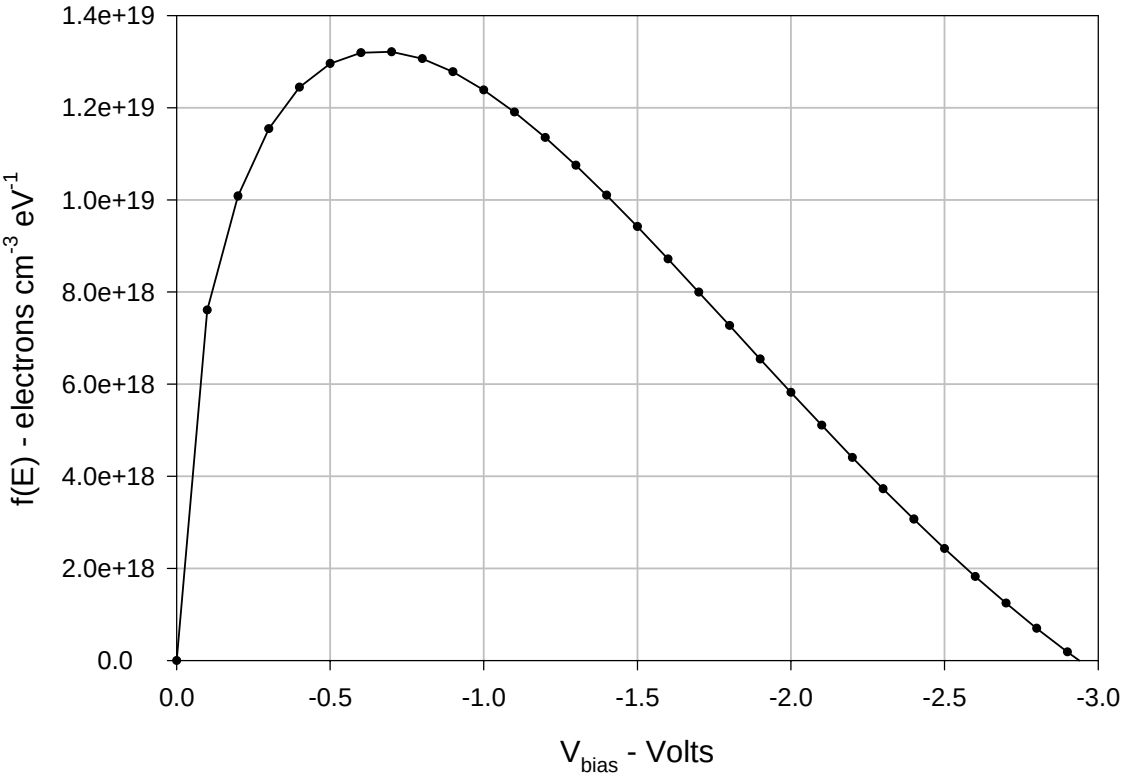
1.4e+19
1.2e+19
1.0e+19
8.0e+18
6.0e+18
4.0e+18
2.0e+18
0.0
f(E) - electrons cm-3 eV-1
0.0
-0.5
-1.0
-1.5
-2.0
-2.5
-3.0
Vbias - Volts

Figure 5